

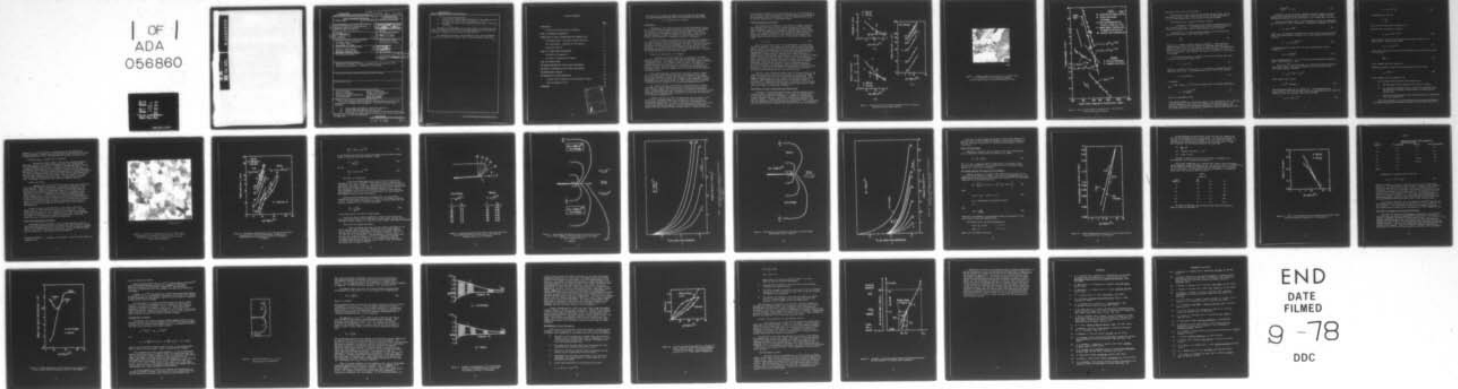
AD-A056 860

SOUTHWEST RESEARCH INST SAN ANTONIO TEX  
CRACK TIP PLASTICITY ASSOCIATED WITH CORROSION ASSISTED FATIGUE--ETC(U)  
MAY 78 D L DAVIDSON, J LANKFORD  
SWRI-02-4268

F/G 11/6  
N00014-75-C-1038  
NL

UNCLASSIFIED

1 OF 1  
ADA  
056860



END  
DATE  
FILMED  
9-78  
DDC

AD NO. \_\_\_\_\_

DDC FILE COPY

AD A 056860



UNCLASSIFIED

SECURITY CLASSIFICATION OF THIS PAGE (When Data Entered)

- ↓
- 4) strain range distributions ;  
the effect of a water vapor environment on the energy required to form a unit area of new crack surface; *and delta*
  - 5) the effect of cyclic stress intensity factor ( $\Delta K$ ) on the above variables.

Throughout the development of the above results, an effort has been made to correlate the results of other investigators with the present experimental findings, and to present unifying concepts.

The mechanism of fatigue crack propagation in an inert environment is given, and the effect of water vapor on that mechanism is described.

↑

SECURITY CLASSIFICATION OF THIS PAGE (When Data Entered)

TABLE OF CONTENTS

	<u>Page</u>
INTRODUCTION	1
Criteria For Dislocation Cell Formation	1
CRACK TIP SUBGRAIN DISTRIBUTION	2
CORRELATIONS OF CYCLIC STRESS RANGE AND SUBGRAIN SIZE	2
The Subgrain Size - Dislocation Density Relation	6
The Stress Range - Subgrain Size Correlation	9
Strain Rate Effects	9
CRACK TIP STRESS RANGE DISTRIBUTION	9
The Effect of Changing $\Delta K$	12
The Effect of Changing Environment	12
CRACK TIP STRAIN RANGE	18
THE ENERGY REQUIRED FOR FATIGUE CRACK PROPAGATION	18
THE EFFECT OF HYDROGEN ON FLOW STRESS AND FRACTURE	22
INTERPRETATION OF RESULTS	24
THE MECHANISM OF CRACK PROPAGATION	28
Fatigue Crack Propagation (No Environmental Effect)	30
The Environmental Effect	30
REFERENCES	33

ACCESSION for	
NTIS	Write Section <input checked="" type="checkbox"/>
DDC	Buff Section <input type="checkbox"/>
UNANNOUNCED	
JUSTIFICATION	
BY	
DISTRIBUTION/AVAILABILITY CODES	
DTIC	DTIC
A	

FATIGUE CRACK TIP STRESS AND STRAIN RANGE DISTRIBUTIONS, THE ENERGY FOR CRACK PROPAGATION AND THE EFFECT OF WATER VAPOR ON THESE FACTORS

D. L. Davidson and J. Lankford

Introduction

A knowledge of the stress, strain, and energy distributions around the tip of a fatigue crack would be helpful in understanding the response of the material to the remotely applied loading conditions, both for the condition of environmental interaction and without. Then from the material response, it might be possible to either predict the rate of fatigue crack propagation or improvise a method of retarding it.

To this end, Davidson and Lankford<sup>(1)</sup> have utilized the propensity of low carbon steel to form a dislocation cell structure near the crack to calculate the energy required to propagate the crack. From this calculation, the spacial distribution of absorbed energy around the crack may also be determined. It is the purpose of this paper to extend the use of the experimentally measured dislocation cell structure distribution to estimate the stress distribution in the near crack region.

Criteria for dislocation cell formation

Dislocation cellular structures, or subgrains, form within the grain structure of low carbon steel upon the attainment of a critical dislocation density. The number of cycles  $N$  required for subgrain formation is dependent on the level of shear strain per cycle. The details of subgrain formation are different on the surface and in the interior, but once the critical dislocation density is achieved, and subgrains form, continued cycling causes the subgrain size to decrease to an approximately equilibrium value.

For a smooth specimen cycled between controlled limits of plastic strain, giving a plastic strain range  $\Delta\epsilon_p$ , the resulting stress range,  $\Delta\sigma$ , at first changes relatively fast and finally reaches an approximately equilibrium value (but oscillations of unknown origin sometimes do occur). Attainment of an equilibrium stress for this loading condition is thought to coincide with the formation of an equilibrium subgrain size.<sup>(2,3)</sup>

For a smooth specimen cycled between controlled limits of stress, resulting in a range of applied stress,  $\Delta\sigma$ , the plastic strain range at first increases rapidly and finally reaches an approximate equilibrium value, although subsequent small oscillations in this value have been found<sup>(4)</sup>. Attainment of an equilibrium  $\Delta\epsilon_p$  is thought to coincide with the formation of an equilibrium subgrain size.

Likewise, the work per cycle, as measured by the area within a plot of  $\Delta\sigma$  vs  $\Delta\epsilon_p$ , increases rapidly with cycling, and finally attains an approximately equilibrium value which is believed to coincide with an equilibrium subgrain size. It is this last effect which allowed calculation of the energy of crack propagation to be determined from the measured subgrain size distribution around a fatigue crack.<sup>(1)</sup> Subgrain sizes may

also be used as a measure of stress distribution due to the attainment of an equilibrium value of stress under strain controlled cycling, and may be used to measure strain distribution if a way of summing  $\Delta\epsilon_p$  over N can be found to obtain total or accumulated strain.

#### Crack Tip Subgrain Distribution

The distribution of subgrains in the wake of a fatigue crack has been measured for a range of cyclic stress intensities ( $\Delta K$ ), both for crack propagation in an inert environment (nitrogen with 1 ppmv water vapor) and in an aggressive environment (12,000 ppmv water vapor or 50% R.H.). The subgrain distribution was determined, using the electron channeling contrast technique (5), and resulted in the finding of a linear relation between subgrain size, d, and distance from the crack, r. (6)

$$d = A + Br \quad (1)$$

There is statistical scatter in the measurement of A and B from specimen to specimen. The reasons for this scatter are partially known. Clearly, there is an interaction between the crack tip stress field and the local grain orientations near the crack which has some random nature. Microscopically, the crack deviates from growth perpendicular to the loading axis, thereby causing a changing mix of mode I and mode II opening as the crack advances, which is known to alter the crack tip stress field. The data currently available, Figure 1, for the intercept A, slope B, and extent of subcell formation  $r_1$ , suggests that the presence of water vapor causes the subgrain size near the crack plane to undergo alteration as  $\Delta K$  increases, whereas an inert environment does not. For both environments, increasing  $\Delta K$  causes the slope B to decrease, with B for the water vapor environment decreasing faster than for the dry environment. More data is required for a refinement of quantitative details of these observations, but the trends are clear.

Equation 1 also correlates subgrain size with distance ahead of the crack tip, but data in this region is the result of a decreased number of cycles, and may be the result of a nonequilibrium subgrain size. The change in subgrain size also occurs over a much shorter distance in the crack tip region making the slope difficult to determine, except by averaging (i.e., between the subgrain size at the crack tip and the grain size). The size and shape of the subgrain forming region near the crack tip is also known, as illustrated in Figure 2.

#### Correlations of Cyclic Stress Range and Subgrain Size

The number of published research results relating subgrain size to stress, strain, or energy dissipation is not large, but several pieces of excellent work have been accomplished. A summary of the available results is shown in Figure 3. The work of Lawrence and Jones (4), by far the most complete, is complemented by that of Chopra and Gowda (7), and the one experimental point from Davidson and Lankford. (1) It is interesting that the results of Herz, Mughrabi and Wilkens (8) while not quantitatively

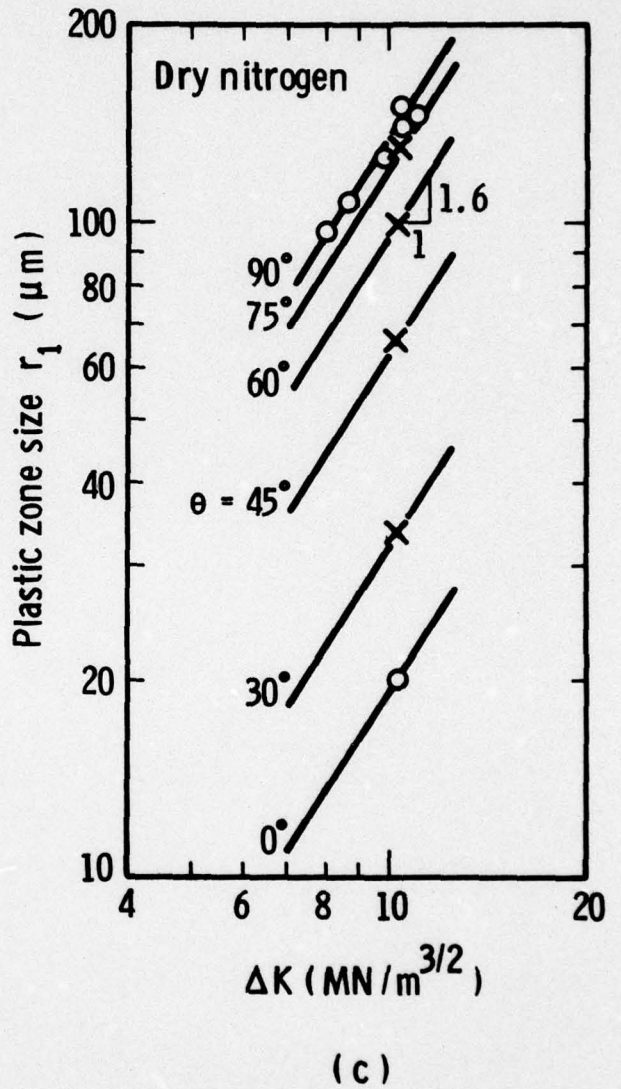
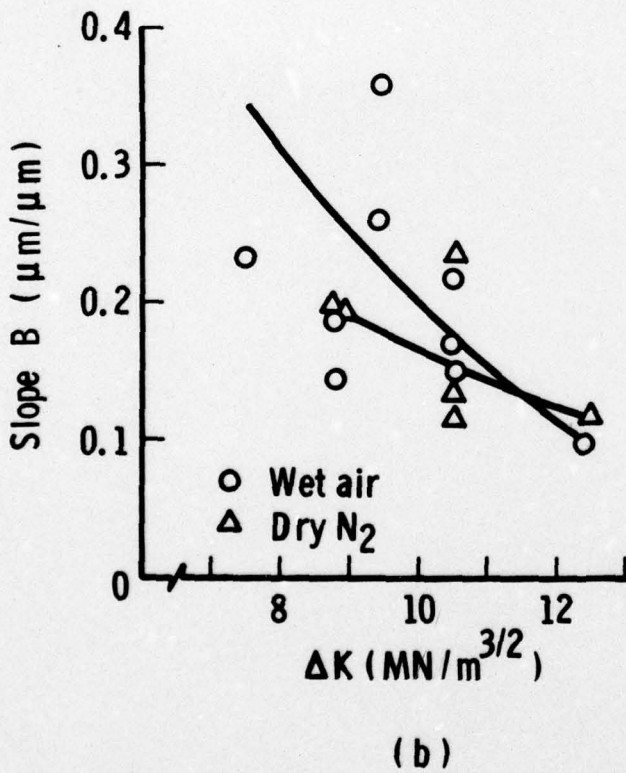
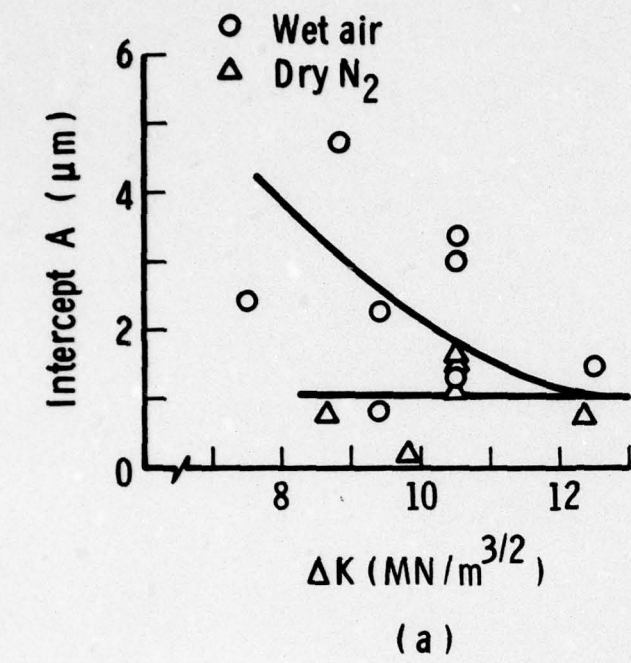
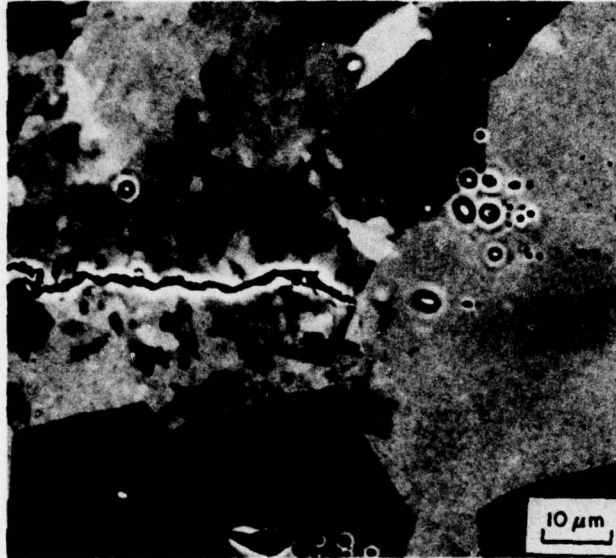


Figure 1. The Effect of Cyclic Stress Intensity Factor on Various Experimentally Derived Variables



1000X

Figure 2. Subgrain Formation At the Tip of a Fatigue Crack.  
 $\Delta K = 10 \text{ MN/m}^{3/2}$ , Dry Nitrogen Environment.  
Section Taken At About 0.1 mm From Specimen Surface.

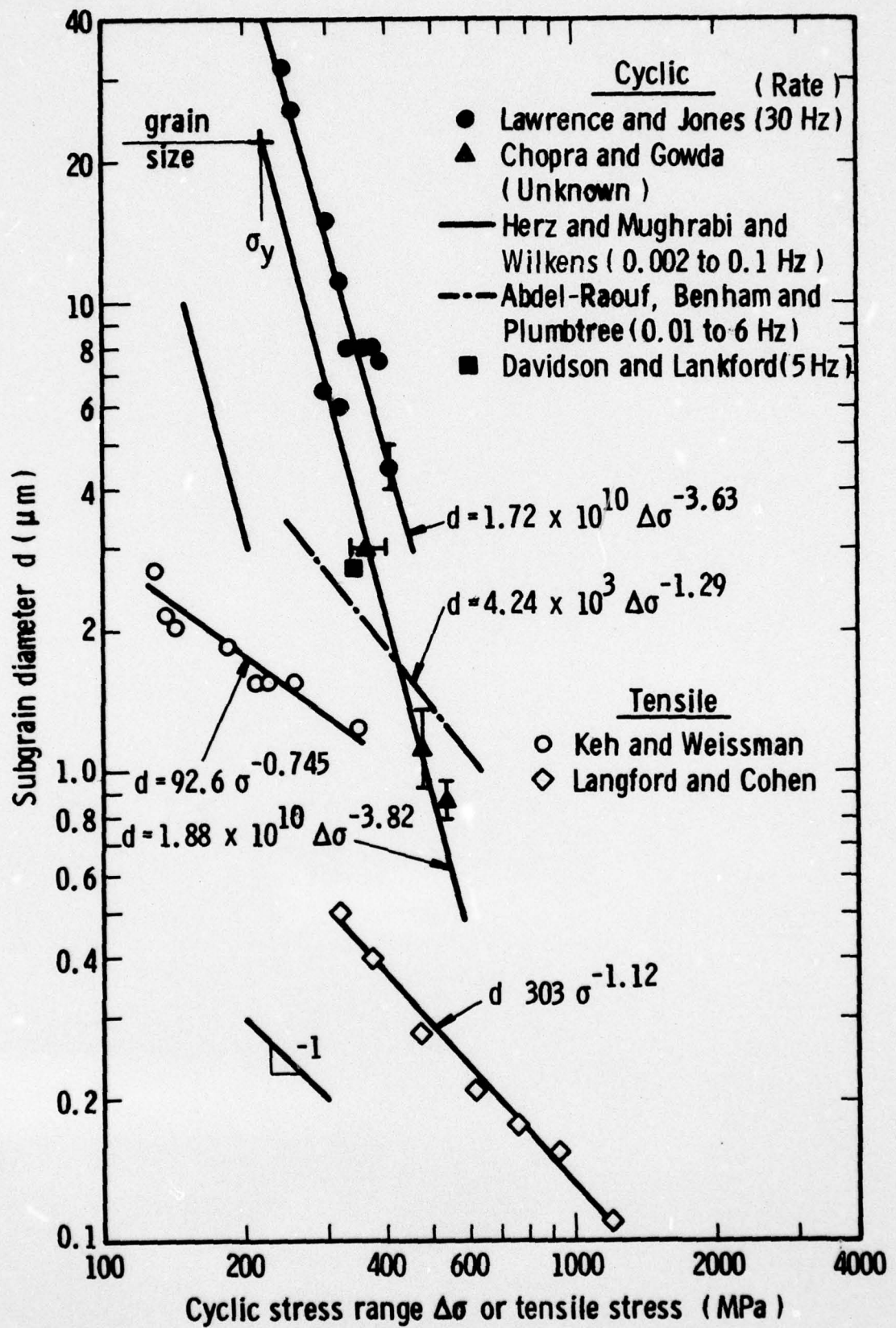


Figure 3. Cyclic Stress Range Vs Subgrain Size. Also Shown Is Data From Monotonic Loading.

equivalent, have about the same slope.\*

The results for tensile testing have neither the same slope, nor the same range of subcell size, except for the work of Keh and Weissman, which is in the same range as part of the results of Chopra and Gowda.

The subgrain size - dislocation density relation

Questions of interpretation arose during the examination of data for inclusion in Figure 3. By examining the relation between dislocation density and subgrain size, some of these questions can be resolved.

Experimentally, the relation between subgrain size and dislocation density has been found by many investigators to be

$$\rho = \frac{K_0}{d^2} \quad (2)$$

where  $K_0$  is a constant (probably material dependent). From theoretical considerations, dislocations are expected to rearrange themselves into periodic clusters once a critical density has been achieved. The mathematical model for this process was developed by Holt,<sup>(9)</sup> and it predicts the relation of equation (2). This relation will thus be considered as a basic physical relation.

For tensile deformation, a relation may be derived between the shear strain and the dislocation density<sup>(10)</sup>

$$\gamma - \gamma_0 = K_1 \sqrt{\rho} \quad (3)$$

where  $K_1$  = a material constant, and  $\gamma_0$  is a constant of integration, which physically may be zero. By combining equations (2) and (3) the relation

$$\gamma d = K_2 (\text{constant}) \quad (4)$$

is obtained.

Abdel - Raouf, et al<sup>(2)</sup> found, through strain rate change experiments, that

$$d = .675 \left( \frac{\Delta \epsilon p}{Z} \right)^{-0.2} \quad (5)$$

which, by rearranging, gives

\* The results plotted are saturation stress  $\sigma_s$ , even though Herz, et al, find the athermal component of the cyclic flow stress  $\sigma_{SG}$  to correlate better. For the strain rates and strain amplitudes relevant to crack propagation,  $\sigma_{SG}$  is a large portion of  $\sigma_s$ , and should correlate with subgrain size nearly as well.

$$\left(\frac{\Delta\epsilon_p}{2}\right)^{0.2} d = .675 \quad (6)$$

Equations (4) and (6) predict different relations between strain and subgrain size, which may be due to monotonic vs cyclic loading or to the experimental technique used by Abdel-Raouf, et al in their data collection.

By using the Seeger theory of the dependence of stress on temperature and strain rate for cyclic deformation, as expounded by Mughrabi, et al, (11)

$$\tau_s - \tau_{SG} = \alpha G b \sqrt{\rho} \quad (7)$$

where  $\tau_{SG}$  is the athermal component of the stress, and  $\tau_s$  is the saturation stress, and substituting in equation (5), a cyclic stress-strain curve of the form

$$\tau_s - \tau_{SG} = K_3 \left(\frac{\Delta\epsilon_p}{2}\right)^{0.2} \quad (8)$$

is obtained, which fits well with the cyclic stress-strain curve of Landgraf (12)

$$\Delta\sigma = 2K' \left(\frac{\Delta\epsilon_p}{2}\right)^{n'} \quad (9)$$

where (experimentally)  $n' = 0.27$  is the cyclic work hardening coefficient, and  $K' \cong 220$  for this Fe - .05C.

Herz, et al (8) find that there is a correlation between dislocation density and subgrain size and the athermal cyclic stress  $\tau_{SG}$  for pure iron single crystals. They find

$$\rho \propto \tau_{SG}^{1.6} \text{ and } d \propto \tau_{SG}^{-1.4}$$

which leads to the relation

$$d\rho^{.88} \propto \text{constant} \quad (10)$$

This relationship does not fit equation (2). By reinterpreting the data of Herz, et al (8) so that both  $\rho$  and  $d$  are proportional to the saturation stress  $\tau_s$ , then the following relations are obtained

$$d = 2 \times 10^9 \tau_s^{-3.6} \quad (11)$$

$$\rho = 1.1 \times 10^{-6} \tau_s^{7.7} \quad (12)$$

By combining (11) and (12)

$$\rho = \frac{K_4}{d^2}$$

which is of the same form as equation (2).

From the data correlation of Figure 3,

$$d = 1.88 \times 10^{10} \Delta\sigma^{-3.82} \quad (13)$$

which compares well with that derived from the data of Herz, et al, equation (11). Rewriting (13) gives

$$\Delta\sigma = 2.26 \sigma_y d^{-0.26} \quad (14)$$

which, when compared to the cyclic stress-strain curve, equation (9), gives  $n' = 0.26$  and

$$\frac{\Delta\epsilon_p}{2} d = 1 \quad (15)$$

which compares well with equation (4)

Assuming equations (2) and (14) and substituting into (15) gives

$$\rho \approx 10^{-5} \Delta\sigma^{7.7} \quad (16)$$

which compares well with equation (12)

The conclusions drawn from the above analysis are:

- a) The functional form of equation (13) or (14) is correct.
- b) Our analysis of the data of Herz, et al<sup>(3)</sup> is consistent with both the data of Figure 3 and the physical relation given by equation (2).
- c) There is an inconsistency in the correlation given by Abdel-Raouf, et al,<sup>(2)</sup> equation (5).

The self-consistency of the above argument fits with the experimental correlations made previously between work per cycle and subcell size (Ref 1,

Appendix C). It also indicates a consistency between the mechanism of subgrain formation in tensile and cyclic deformation, implies that the concept of Similitude<sup>(10)</sup> is correct, and reaffirms the validity of equation (2).

#### The stress range - subgrain size correlation

The results we have chosen to use for the calculations made in this paper, Figure 3, are shown as the heavy black line connecting the yield stress-grain size point for our material, and passing through the data of Chopra and Gowda, part of that of Lawrence and Jones, and the one experimental point obtained for our material. In effect, we have normalized the data of Lawrence and Jones and Herz and Mughrabi to our grain size material. The reason for using the grain size-yield stress point is that subgrains are known to begin forming at the yield stress. This is illustrated in Figure 4, which shows the material on either side of a Luders front. As may be seen, the passage of the Luders front results in subgrain formation.

#### Strain-rate effects

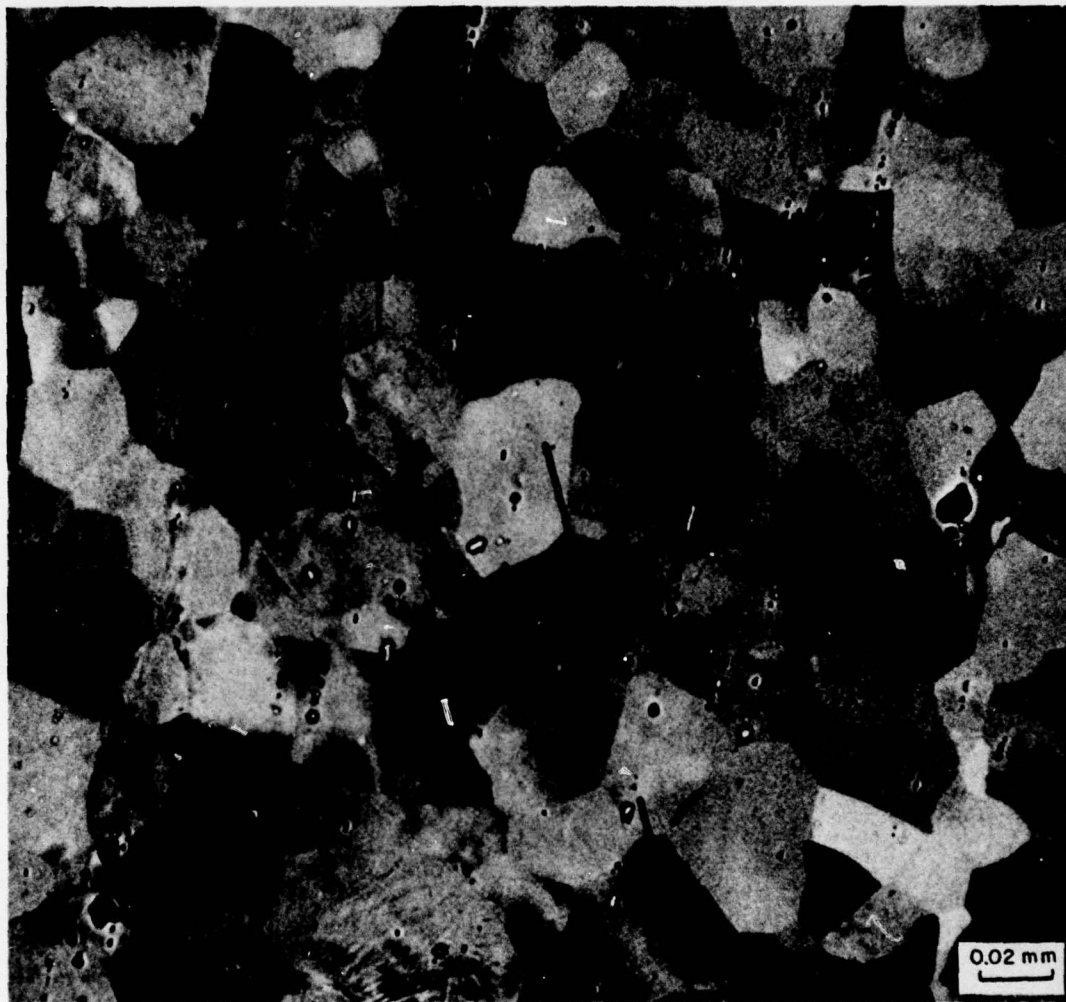
Mughrabi, Herz and Stark<sup>(11)</sup> have clearly shown that strain rate is an important variable in assessing the deformation properties of iron single crystals. Similar work on rate effects for polycrystalline iron has been done by Abdel-Raouf, Behnam and Plumbtree<sup>(2,3)</sup>, which shows the importance of this factor although their results are inconsistent with those of Herz, et al. A comparison of the present experimental results, using a loading rate of 5 Hz (a crack tip strain rate of approximately  $10 \text{ sec}^{-1}$ )\*\* with those previously reported for the same Fe-.05C steel,<sup>(10)</sup> for which the loading rate was 152 Hz\*\* (a crack tip strain rate of approximately  $3 \times 10^2 \text{ sec}^{-1}$ )\*\*, Figure 5, reveals a difference in the extent of plasticity along the crack wake and a difference in the effect of  $\Delta K$  on this plasticity.

Because of these conflicting data on rate effects, the data in Figure 3 have not been corrected to one value of strain rate. For the strains near the crack tip ( $\sim 1$ ), saturation stress range is not thought to be greatly affected by a rate change of 10; thus, the correlation shown in Figure 3 is not expected to be much different between 5 and 50 Hz, which covers most of the data used in the correlation.

#### Crack Tip Stress Range Distribution

Combining the data in Figures 1 and 3, through equations 1 and 14, the stress range distribution near the fatigue crack may be derived. Stress range has been computed around the crack tip for the dry nitrogen environment case for two values of  $\Delta K$ , and for both the dry nitrogen and wet air cases for two values of  $\Delta K$ . The equation for stress range is

\*\* strain rate<sup>(11)</sup> =  $2 \times \text{frequency} \times \text{strain range}$ . Crack tip strain range was assumed to be 1.



Luders Front

Figure 4. Formation of Subgrains in Fe - .05C Steel Due To the Passage of a Luders Front Upon Yielding. The Front Moved From Left to Right, With Material On the Left Having Formed Subgrains.

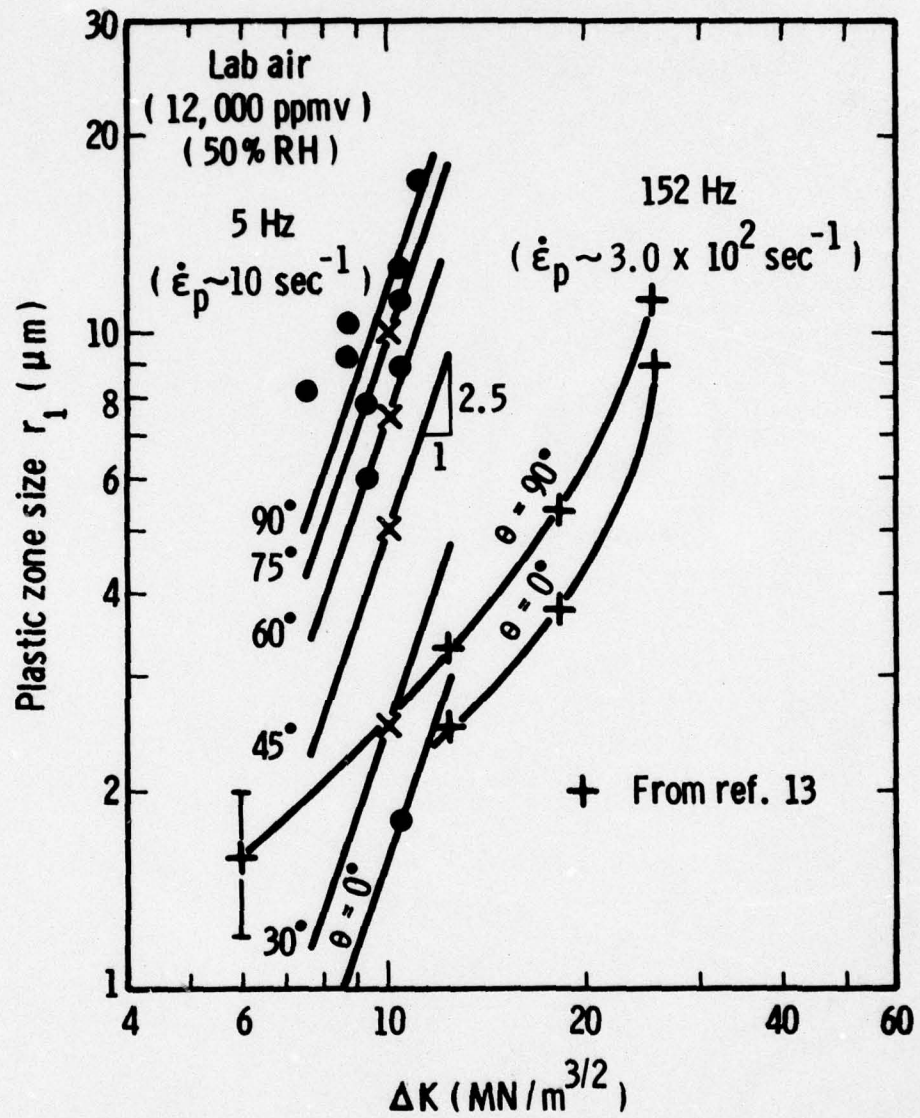


Figure 5. Correlation Between Plastic Zone Size and Cyclic Stress Intensity Factor For Cracks Propagated In Humidity Air (Approximately 50% RH) Showing the Effect of Frequency of Loading.

$$\frac{\Delta\sigma}{\sigma_y} = 2.26(A + Br)^{-0.262} \quad (17)$$

or the distance from the crack tip may be normalized by the factor proportional to the plastic zone size  $(\Delta K/\sigma_y)^2$ , giving

$$\bar{r} = \frac{r}{(\Delta K/\sigma_y)^2} \quad (18)$$

so that

$$\frac{\Delta\sigma}{\sigma_y} = 2.26(A + B\bar{r})^{-0.262} \quad (19)$$

The effect of changing  $\Delta K$

The stress range distribution around the crack tip has been computed for  $\Delta K = 8$  and  $12 \text{ MN/m}^{3/2}$ . The functions used to calculate the distribution are shown in Figure 6. These were derived from the observation that plastic zone shape is described approximately by the plane strain plastic zone calculation as modified by experimental observation near  $\theta = 0^\circ$ .<sup>(1)</sup> The  $\Delta K$  dependence of the plastic zone boundary dimension  $r_1$  was measured experimentally as  $\Delta K^{1.6}$  at  $\theta = 90^\circ$ , and the values at the other angles have been assumed to have the same  $\Delta K$  dependence.

Using the above observations and assumptions, the yield stress normalized stress range distribution is found to be as is shown in Figures 7 and 8. The distribution of stresses is a smooth function having the form given by equations (17) or (19) which approaches

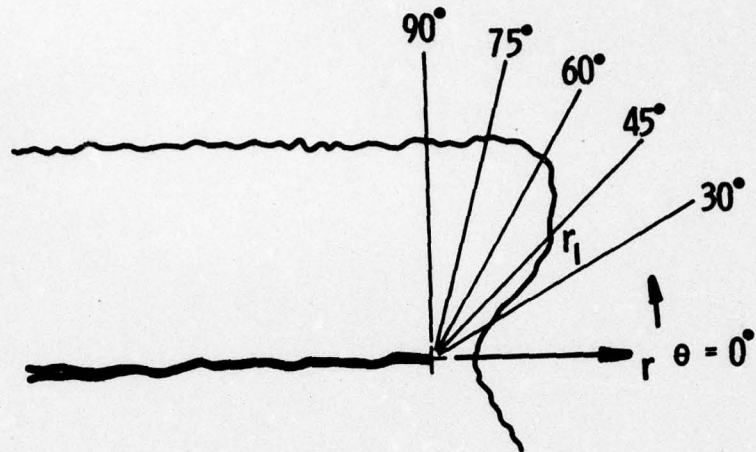
$$\frac{\Delta\sigma}{\sigma_y} = \frac{2.26}{(B\bar{r})^{0.262}} \quad (20)$$

in the outer part of the subcell forming region.

The curves cannot quite be normalized by equation (18) because the data of Figure 1(c) have a  $\Delta K^{1.6}$  dependency instead of  $\Delta K^2$ . thus the curves of Figure 7 cannot be made to lie one on the other using  $\bar{r}$  as the spacial variable.

The effect of changing environment

Since the subcell size near the crack plane is decreased at low  $\Delta K$  for the water vapor environment, the implied cyclic stress range is also decreased, and the stress range distribution is changed, reflecting the fact that the extent of plasticity is related to  $\Delta K$  as  $r_1 \propto \Delta K^{2.5}$  ( $\theta = 90^\circ$ ,  $\Delta K = \text{up to } 13 \text{ MN/m}^{3/2}$ ). The distribution of stress range around the crack tip is shown in Figures 9 and 10, in comparison to the dry nitrogen environment for the same  $\Delta K$ . At the higher  $\Delta K$  ( $12 \text{ MN/m}^{3/2}$ ), the stress range distribution becomes nearly equal for both environments, and appears much as shown in Figure 7.



Dry nitrogen

$$r_i = r_{10} \Delta K^{1.6}$$

$\theta$	$r_{10}$
0°	0.4
30°	0.8
45°	1.5
60°	2.2
75°	3.0
90°	3.4

Wet air

$$r_i = r_{10} \Delta K^{2.5}$$

$\theta$	$r_{10}$
0°	0.05
30°	0.08
45°	0.15
60°	0.23
75°	0.29
90°	0.36

Figure 6. Angular Relations Between Plastic Zone Size and Cyclic Stress Intensity Factor At the Crack Tip For Both Dry Nitrogen and Wet Air Environments.

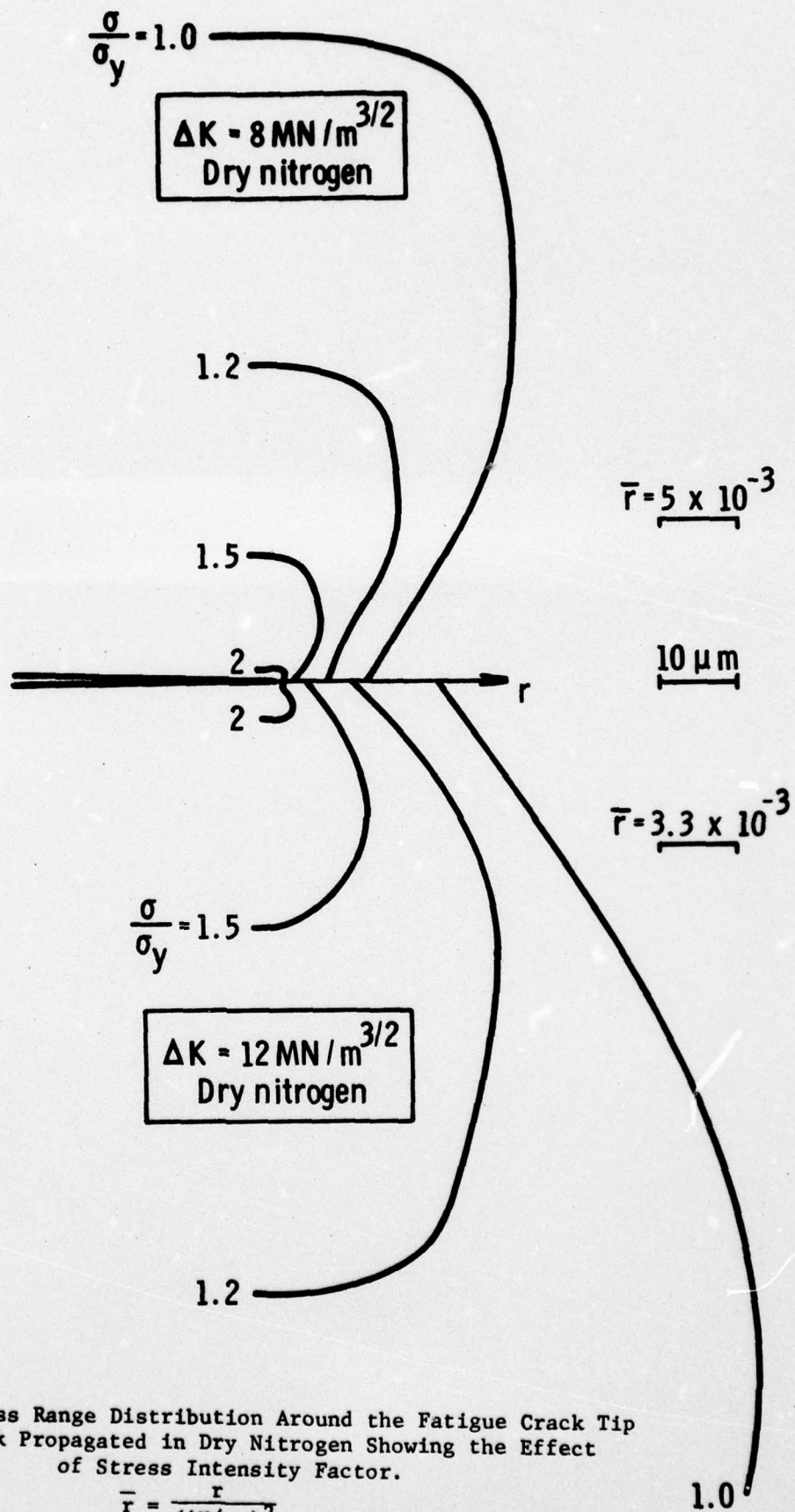


Figure 7. Stress Range Distribution Around the Fatigue Crack Tip For a Crack Propagated in Dry Nitrogen Showing the Effect of Stress Intensity Factor.

$$\bar{r} = \frac{r}{(\Delta K / \sigma_y)^2}$$

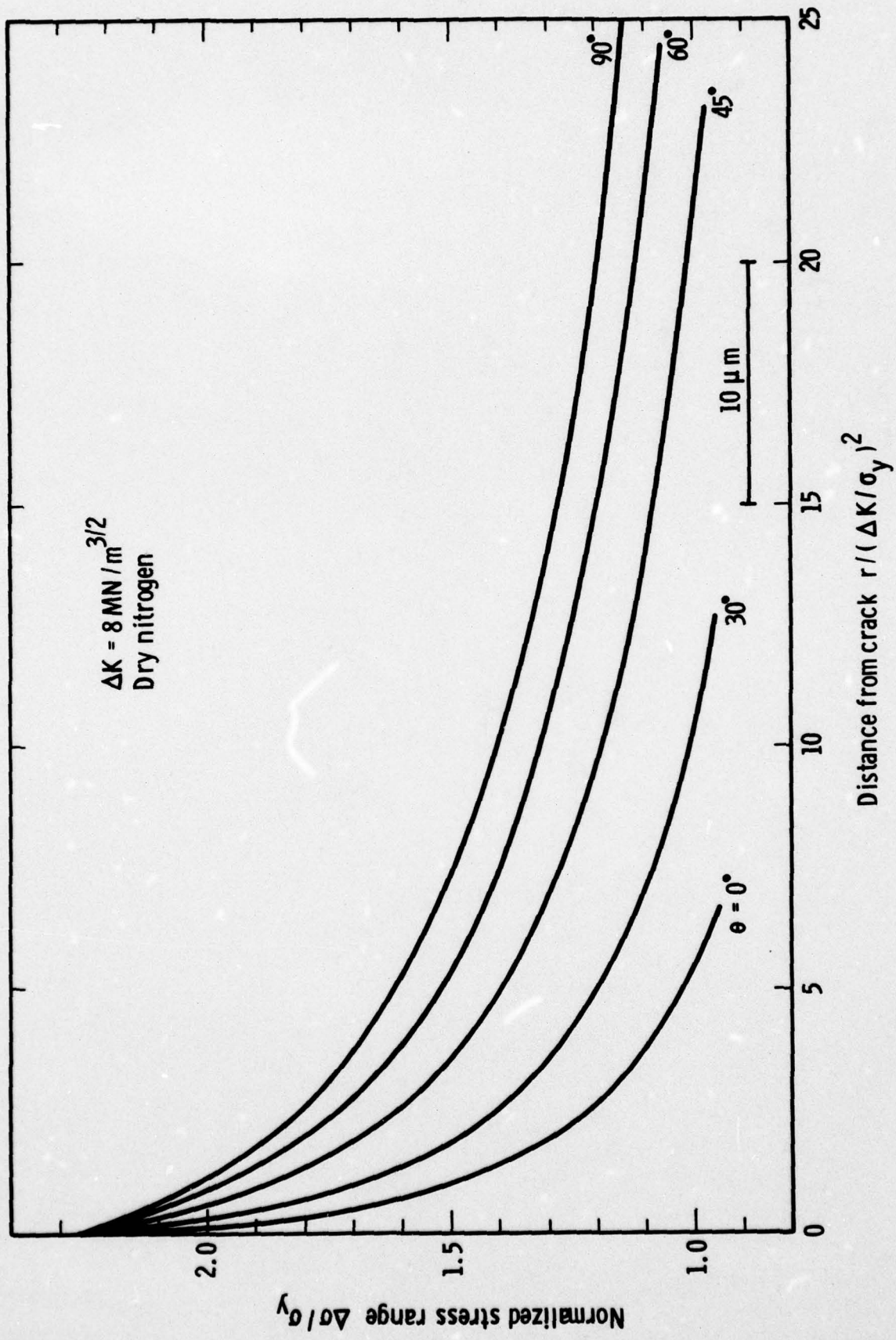


Figure 8. Stress Range As a Function of Distance For Various Angles For a Crack Propagated in Dry Nitrogen At  $\Delta K = 8 \text{ MN/m}^{3/2}$

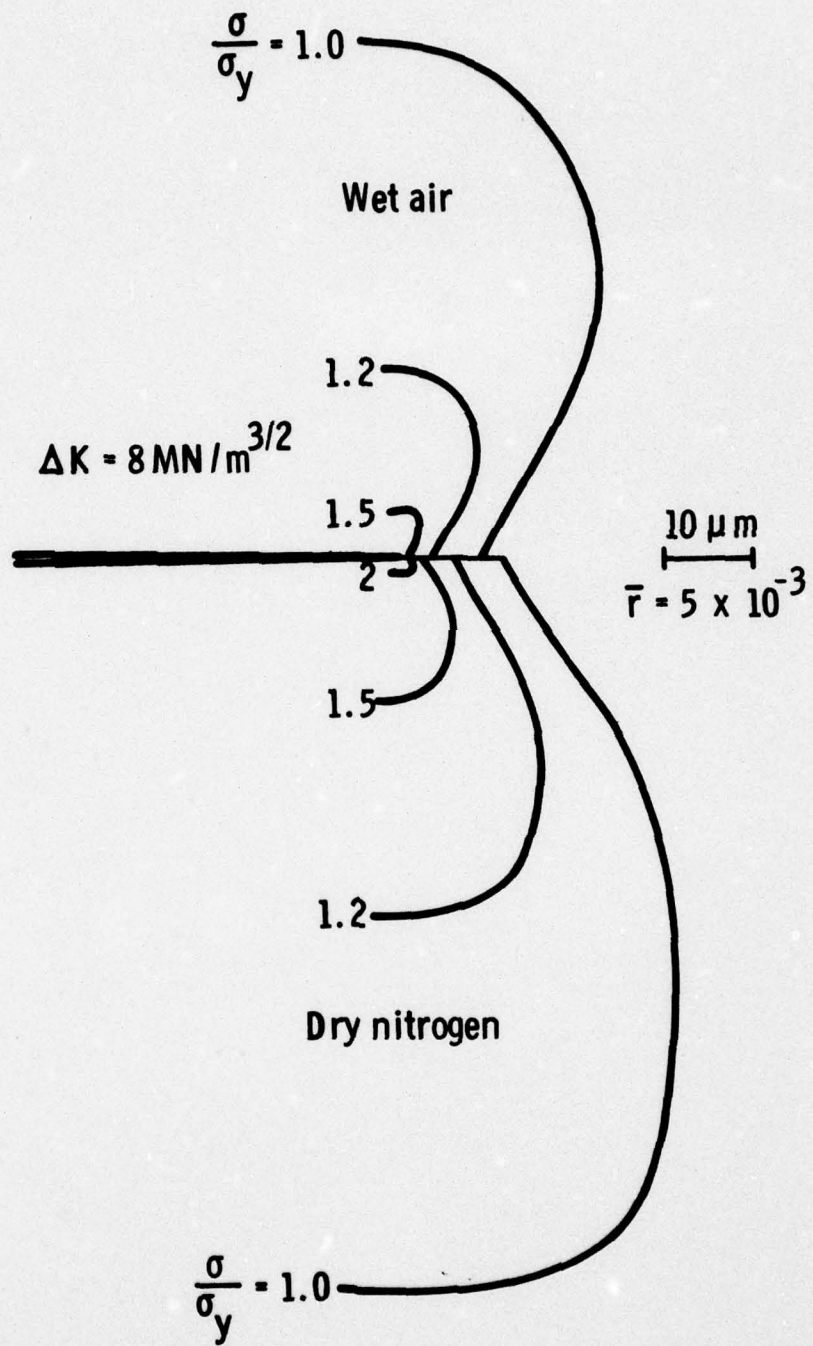


Figure 9. The Effect of Environment on the Crack Tip Stress Range Distribution At  $\Delta K = 8 \text{ MN/m}^{3/2}$

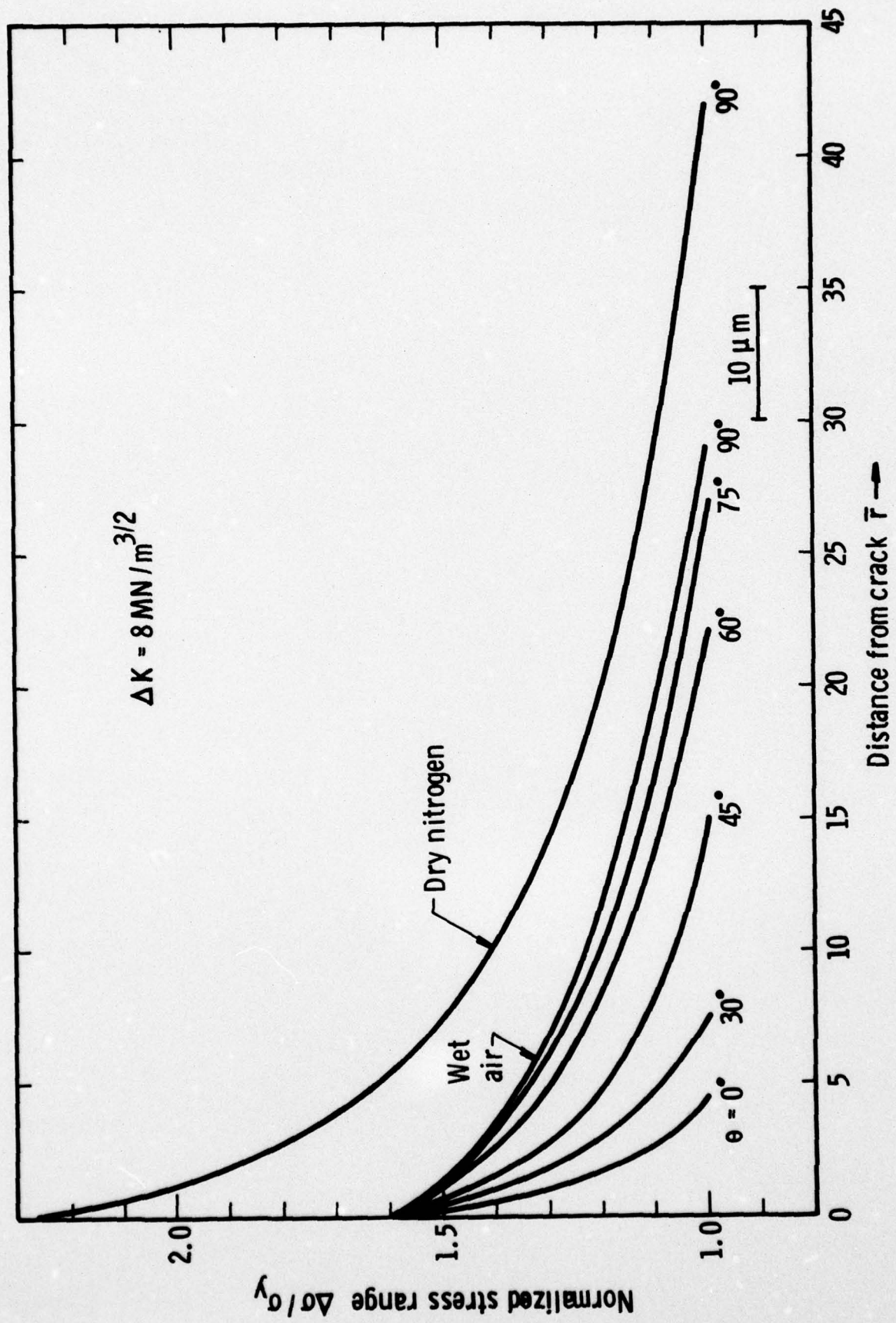


Figure 10. The Effect of Environment On the Angular Distribution of the Stress Range - Distance Relation

The rate of crack propagation has very accurately been measured for the water vapor and dry nitrogen environments, and is shown in Figure 11. Only the resulting statistically fit curves are shown because of scatter in the data.

#### Crack Tip Strain Range

Comparison of equation (14) with that of the cyclic stress-strain curve, yielded the relation given as equation (15), namely

$$\Delta\epsilon_p = \frac{2}{d} = \frac{2}{A + Br} \quad (21)$$

At  $r = 0$ ,  $\Delta\epsilon_p = 2$  (dry nitrogen), irrespective of  $\Delta K$ , and  $\Delta\epsilon_p = 0.53$  (wet air,  $\Delta K = 8 \text{ MN/m}^{3/2}$ ). In the outer portion of the subcell forming region,  $\Delta\epsilon_p \propto \frac{1}{r}$  for both environments.

#### The Energy Required for Fatigue Crack Propagation

Subgrain formation by passage of the crack may also be used to calculate the energy required to create a unit area of new fatigue crack. The methodology for this calculation has been fully explained<sup>(1)</sup> and is generally summarized by the following relations

$$W_T = 2 \left[ \int_0^{r'} W_c(r) N(r) dr + \int_{r'}^{r_1} W_c(r) N(r) dr \right] \quad (22)$$

where

$$W_c(r) = W_{co} d^{-n} \quad \text{and } d = A + Br \quad (23)$$

$W_{co}$  = experimentally determined constant

$n = 1$

and

$$N(r) = \frac{dL}{da/dN} \quad (24)$$

where  $dL$  is the dimension of the material ahead of and parallel to the crack plane in which the subgrains form.

The shape of  $dL(r)$  has been approximated as

$$N(r) = N_0 + N_1(r) \quad 0 < r < r'$$

$$N(r) = N \quad r' < r < r_1$$

where  $r_1$  is the plastic zone size.

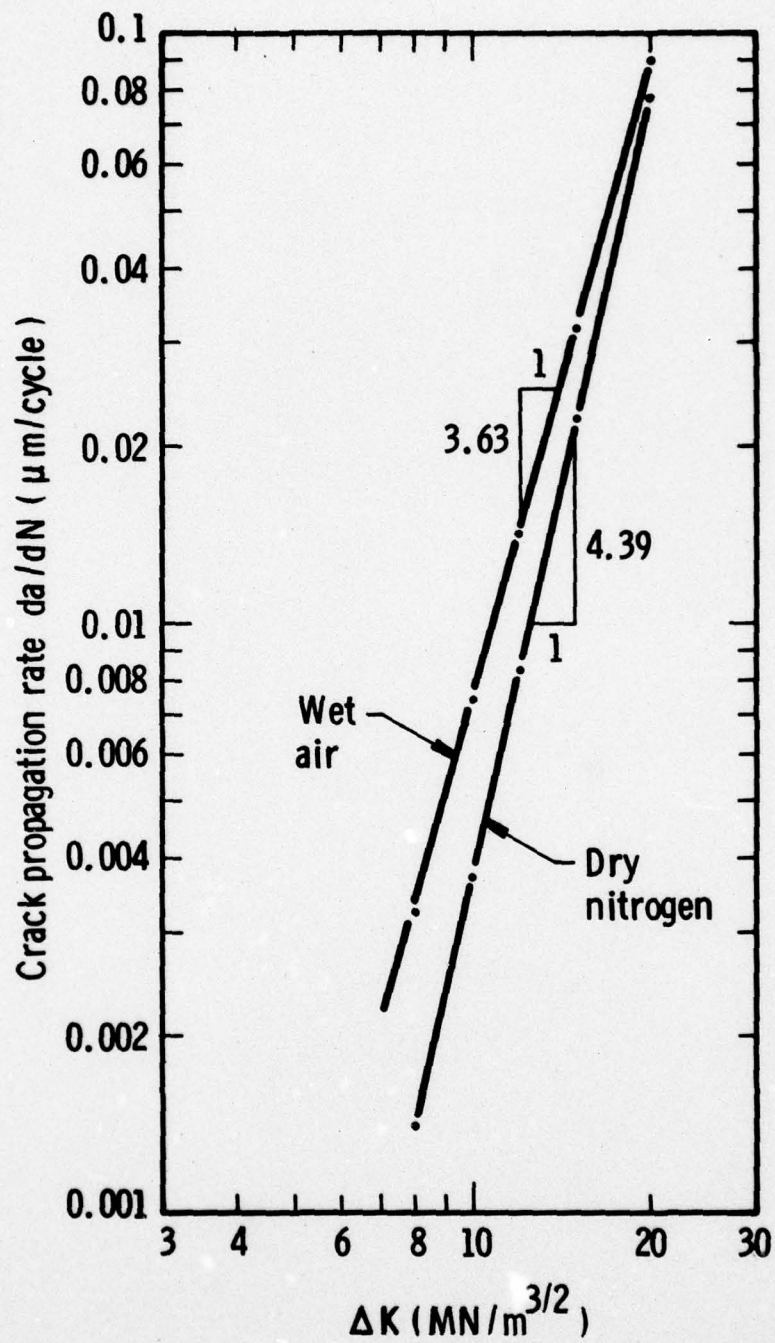


Figure 11. Crack Propagation Rate Vs Cyclic Stress Intensity Factor Showing the Effect of Environment

This methodology has been applied to the data thus far presented for both the dry nitrogen and wet air environments. For values of  $\Delta K$  above 20, the slope of the  $da/dN$  vs  $\Delta K$  is assumed to be 4.0 for both environments. A "limiting case" calculation may be made for  $\Delta K$  above this value. To make this calculation the following assumptions have been made:

- (1)  $\frac{da}{dN} \propto \Delta K^4$
- (2) (plastic zone size)  $r_1 \propto \Delta K^2$
- (3) slope  $B \propto \Delta K^{-2}$

The data of Figures 1(c) and 5 give validity to assumption (2), and assumption (3) is reasonable from Figure 12.

Using these assumptions, the "limiting case" gives a value of fatigue crack propagation energy independent of  $\Delta K$ . For values of  $\Delta K = 8$  to 13  $MN/m^{3/2}$ , for the dry nitrogen environment, experimentally derived values of the exponents and of  $B$  were used. For  $\Delta K$  between 13 and 20, intermediate or "transition" values were used, which are given in Table I.

TABLE I  
Exponents

$\frac{\Delta K}{(MN/m^{3/2})}$	$\frac{da}{dN}$	$r_1$	$B$
8	4.4	1.6	.22
10	4.4	1.6	.16
12	4.4	1.6	.12
14	4.3	1.7	.096
16	4.2	1.8	.071
18	4.1	1.9	.071

For both environments, the resulting energy values calculated are shown in Figure 13 and Table II.

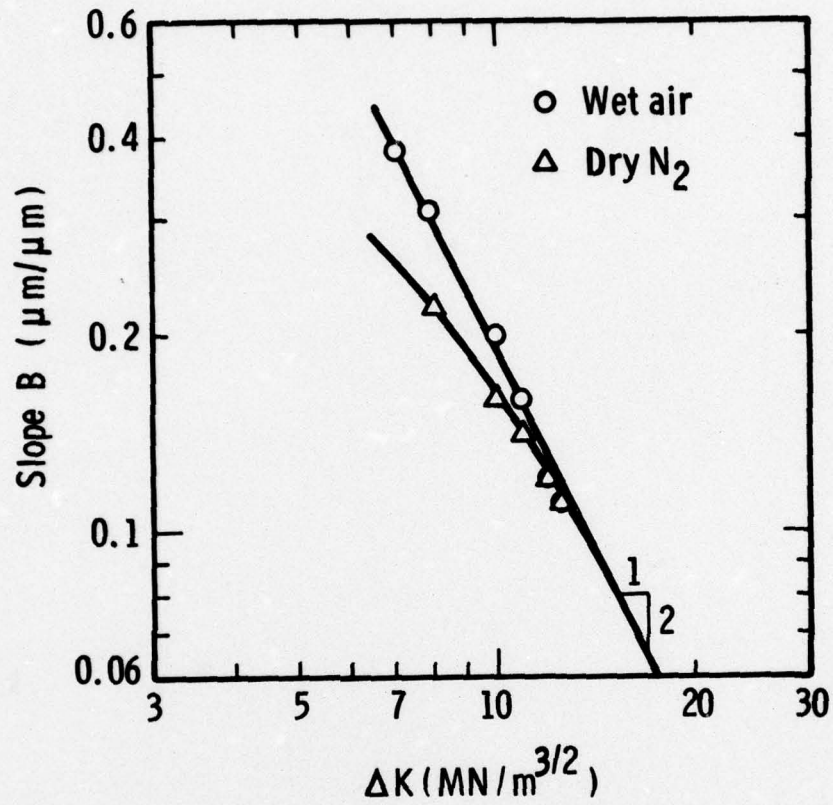


Figure 12. Slope of the Subgrain Size Distribution (B) Vs Cyclic Stress Intensity Showing the Approach to a Limiting Slope

TABLE II

$\Delta K$ MN/m <sup>3/2</sup>	<u>Energy for Fatigue Crack Propagation</u> (10 <sup>5</sup> Joules/meter <sup>2</sup> )		
	<u>Dry Nitrogen</u>	<u>Wet Air</u>	<u>Due to Environment</u>
8	17.1	1.5	15.6
10	12.5	2.4	10.1
12	9.9	4.1	5.8
14	10.8	9(est)	1.8
16	14.1	14(est)	0
18	21.1		
LIMIT	25		

Parametrically, equation (22) has the form

$$W_T \propto C_1 \Delta K^{-p} + C_2 \Delta K^{-q} \quad (25)$$

where the exponents  $p$  and  $q$  are dependent on the values of those shown in Table I. The reason Region I (dry nitrogen) of Figure 13 has a negative slope is because the slope of  $da/dN$  vs  $\Delta K$  has a slope greater than 4; conversely, for the wet air environment the exponent is 3.63 and the slope of the curve in Figure 13 is strongly positive. The magnitude of  $W_T$  in equation (25) is also dependent on  $C_1$  and  $C_2$  which are proportional to  $B$ ; thus, the existence of Region II, or transition region between Region I, the threshold region, and the limiting region depends very strongly on the interrelationships between the actual values of the constants chosen.

The previous calculation of crack propagation energy<sup>(1)</sup> found for dry nitrogen  $W_T = 17.3 \times 10^5$  J/m<sup>2</sup> and for wet air  $W_T = 5.7 \times 10^5$  J/m<sup>2</sup>, both at  $\Delta K = 10$  MN/m<sup>3/2</sup>. The values shown in Table II are somewhat different, and reflect greater accuracy in the determination of crack propagation rate.

#### The Effect of Hydrogen on Flow Stress and Fracture

The effect of hydrogen on the mechanical properties of iron and iron alloys has been the subject of considerable recent effort. The work of Karpenko, Yarmchenko and Shved<sup>(14)</sup> showed that for Armco Iron ( $7 \times 10^{-3}$  wt % C), hydrogen charging increased the yield strength from 296 to 336 MPa when samples were thin enough to obtain hydrogen charging completely through the specimen thickness. Likewise, the tensile ductility was reduced by hydrogen charging during testing. Asano and Otsuka<sup>(15)</sup> examined a decarburized mild steel ( $5 \times 10^{-4}$  C) and found essentially the same results as Karpenko,

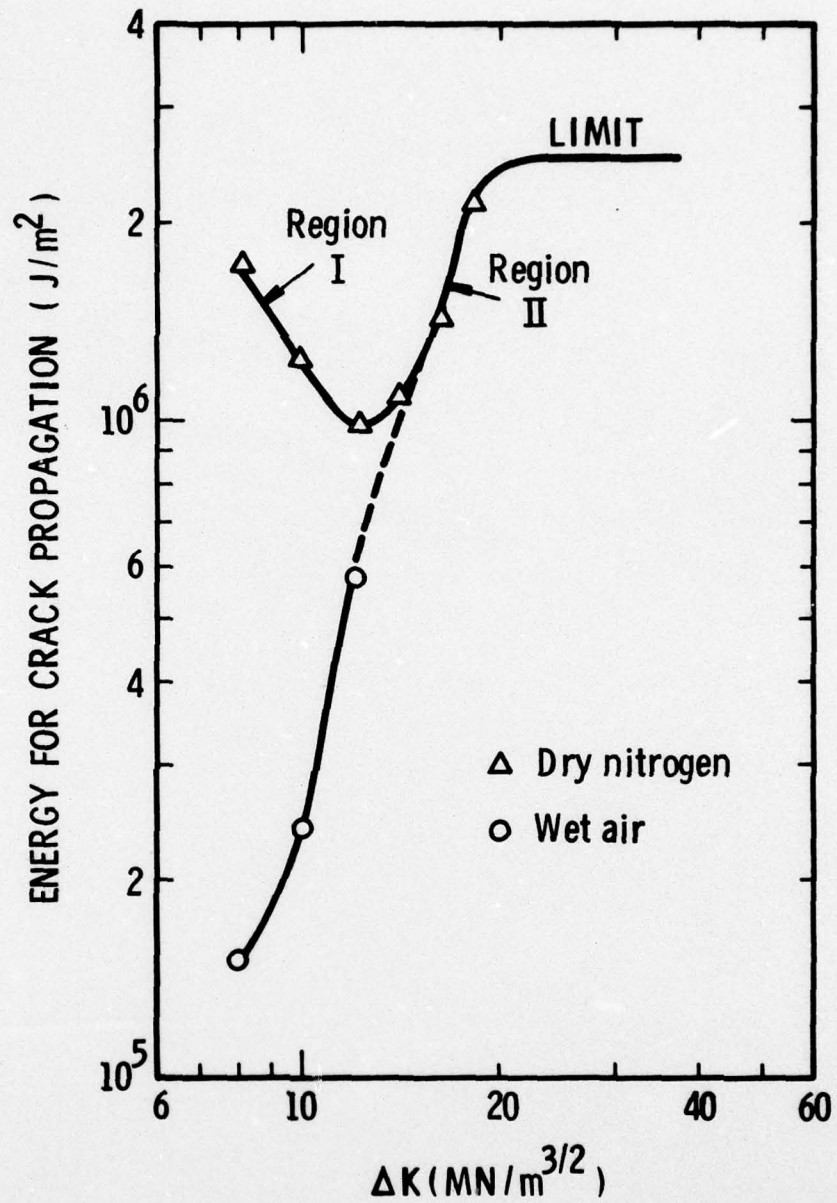


Figure 13. Energy Required For Crack Propagation As a Function of Cyclic Stress Intensity Showing the Effect of Environment

et al, at least qualitatively.

Using ultra high purity iron ( $3 \times 10^{-5}$  C), Kimura, Matsui and Moriya<sup>(16)</sup> found that hydrogen charging resulted in a decrease in flow stress, contrary to the above cited results. Bernstein<sup>(17)</sup> reported French work, also on high purity iron, which showed a decrease in flow stress due to hydrogen.

Lunarska, et al<sup>(18)</sup> have measured by torsion pendulum the shear modulus of high purity iron (5 ppm nonmetallic impurities) and concluded that hydrogen charging decreases the shear modulus, and that this is related to a reduction in the lattice cohesive strength.

The conclusions to be drawn from these studies are that the carbon content of the iron is an important factor in whether the flow stress is increased or decreased by hydrogen. For Fe - .05C steel, then, hydrogen charging is expected to increase the flow stress. Quantitatively the effect should be about that found by Karpenko, et al, or about a 13% increase, assuming saturation. Hydrogen charging also lowers the tensile ductility of steel, probably through its reduction in cohesive strength.

#### Interpretation of Results

The shapes of the crack tip subcell forming regions observed for this material are very much like those graphed by Schijve<sup>(19)</sup> who derived asymptotic solutions for the elliptic hole-in-a-sheet solution of Timoshenka and Goodier. The plain strain solutions for the shear stresses

$$\tau_2 = \frac{S_1 - S_3}{2} \quad \text{and} \quad \tau_3 = \frac{S_2 - S_3}{2}$$

are

$$\tau_2 = 1/2 S \frac{\sqrt{C}}{2r} \sin \theta \quad \text{and} \quad \tau_3 = 1/2 S \frac{\sqrt{C}}{2r} \cos \frac{\theta}{2} (1 - 2\nu + \sin \frac{\theta}{2})$$

where  $S_i$  are the principal stresses, with  $S_1$  and  $S_2$  in the specimen plane and  $S_3 = \nu(S_1 + S_2)$  out of plane. Figure 14 shows Schijve's results.

Since subgrains form due to the attainment of a critical dislocation density, and dislocations are formed by shear, the stress range which has been calculated and is shown in Figures 7 thru 10 is probably a shear stress range. The asymptotic solutions which have been derived are of the wrong spacial form, since they predict a stress singularity at the crack tip, but their angular form appears to be correct. Ahead of the crack tip,  $\theta = 0^\circ$ ,  $\tau_3 > \tau_2$  gives a finite value to the plastic zone in that region, which  $\tau_2$  does not. Thus, the subgrain forming region is probably due to the maximum shear stress range experienced by the material.

It is not possible to correlate the subgrain size distributions as measured and graphed in Figure 1 with those of other investigators because no other similar data have been found covering the whole plastic zone.

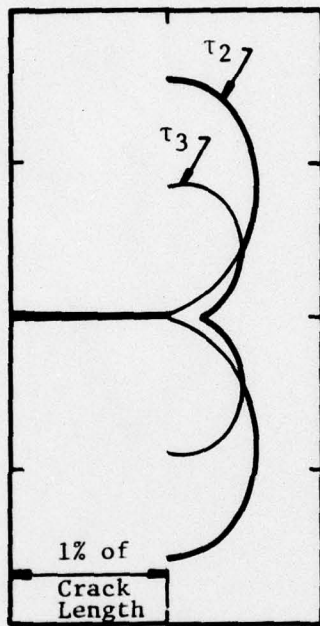


Figure 14. Isostress Lines For  $\tau_2 = \tau_3 = 2S$   
After Figure B5 of Schijve<sup>(19)</sup>

There have been several transmission electron microscopy investigations into subgrain formation near fatigue crack tips in iron and low carbon steel<sup>(20, 21, 22)</sup> which do indicate that subgrains of a minimum size of 0.8 to 1.5  $\mu\text{m}$  are found adjacent to the crack plane for values of  $\Delta K \approx 15 \text{ MN/m}^{3/2}$ . At higher  $\Delta K$  ( $\sim 35 \text{ MN/m}^{3/2}$ ) smaller subgrains ( $\sim 0.5 \mu\text{m}$ ) may form.<sup>(21)</sup>

The spacial form of the crack tip stress distribution shown by Rice and Johnson<sup>(23)</sup> in their Figure 4(a) is (as pointed out by Schwalbe<sup>(24)</sup>)

$$\sigma/\sigma_y = \frac{0.3}{0.1 + \bar{r}} \quad (26)$$

where  $\bar{r} = r/(\Delta K/\sigma)^2$ .

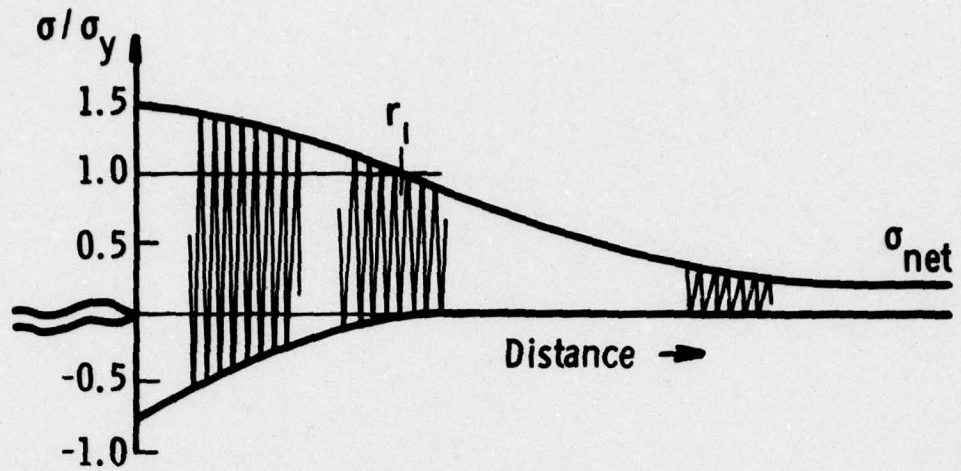
This equation has almost the same form as equation (19) and it does not predict a singularity at the crack tip. Rice and Johnson determined the data to which equation (26) was fitted by finite element analysis of a monotonically loaded crack for a non-work hardening material; the similarity between their calculation and equation (19), which was determined experimentally for a cyclically-hardening material, is thus remarkable.

As commented on by Rice,<sup>(25)</sup> a small volume of material near the tip of an unloaded fatigue crack tip experiences compressive stresses. This point was further amplified by Hahn, et al<sup>(26)</sup> in their etch studies of fatigue crack propagation in Fe - 3 Si. The schematic of the cyclic history of the material ahead of a fatigue crack tip tip (their Figure 14) drawn in terms of strain range fits well the result expressed by equation (21)

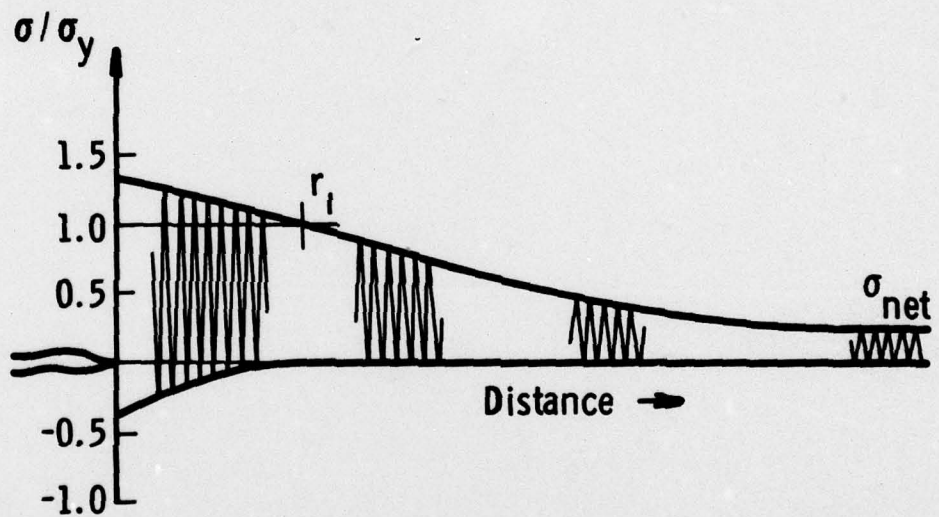
$$\Delta\epsilon_p = \frac{2}{A + Br} .$$

The corresponding expected stress response of the material is shown schematically in Figure 15 for both the dry nitrogen and the wet air environments. For most of the cycles which an element of material experiences as the crack approaches, the stress is positive, but when the crack tip is very close, the large strain amplitude experienced by the material requires compressive stresses to obtain the crack closure observed. Since the strains at the crack tip for the wet air environment are less than those for the dry nitrogen environment, lower compressive stresses are required. The existence of crack tip compressive stress has been demonstrated experimentally by Aira and Tanaka<sup>(27)</sup> who found an increase in amplitude with increasing  $\Delta K$ . Since their measurements were made in "laboratory air", these observations are consistent with our finding that the stress range increases with increasing  $\Delta K$  for the water vapor environment (for  $\Delta K$  up to about  $13 \text{ MN/m}^{3/2}$ ).

There is no direct evidence for the assumption that a wet air environment lowers the compressive stresses in the unloaded state, as compared to the dry environment, but there is indirect evidence. Jono, et al<sup>(28)</sup> have directly observed, at high resolution, cyclically loaded crack tips in grains of Fe - 3 Si oriented to shear only in-plane which were propagated in vacuum and in "laboratory air" environments. In the vacuum environment, the



(a) Dry nitrogen



(b) Wet air

Figure 15. Schematic Representation of the Stress Range Experienced by Material Ahead of the Crack Tip Showing the Effect of Environment.

crack is found to open first behind the crack tip, with the crack opening progressing towards the tip as the load is increased, whereas after being cycled in the laboratory air environment, the crack begins opening at the crack tip. The authors attribute this behavior to crack "rewelding" in the vacuum environment, but our interpretation of this finding is that the crack tip compressive stress magnitude is greater in the vacuum. The direct observations by Jono, et al also support our finding of a decreased strain amplitude at the crack tip due to the presence of water vapor while cycling. Careful examination of their crack tip photographs by a stereoviewing technique<sup>(29)</sup> which allows visualization of crack tip displacements, indicates that more pronounced shear bands with higher strain magnitude exist for the vacuum environment than for the wet air environment. The crack tip is rounder, and the crack tip opening displacement (CTOD) for a value of  $K_{max}$  is greater, Figure 16, for the wet air environment. The change in hysteresis of CTOD with change of environment implies that the near-crack-tip material also undergoes less hysteresis in the water vapor environment, which is in agreement with the calculated energy for crack propagation.

Several investigators have found that water vapor in the environment causes a change in the mode of crack tip opening. Schijve<sup>(30)</sup> has observed a change in mode from a predominantly "shear" to a "tensile" mode on going from a vacuum to humid air environment in 2024 and 7075 aluminum alloys. Davidson and Lankford<sup>(6)</sup> previously reported a similar result for Fe - .05C steel. These observations generally agree with a decreased size of the plastic zone for the crack propagated in wet air<sup>(6)</sup>, and with the present finding of decreased crack tip plastic strain and stress range for these conditions.

#### The Mechanism of Crack Propagation

From the data so far gathered in this investigation, coupled with the findings of other investigators, the effects of a water vapor environment on fatigue crack propagation in low carbon steels at low  $\Delta K$  are as follows:

- 1) The mode of crack propagation is changed from a mix of mode II (shear) + mode I (tensile), where mode II predominates, to a mix of cracking involving more mode I opening. The shape of the crack tip probably changes also.
- 2) The intensity of the shear band strain is decreased by there being more bands operative having lower strain.
- 3) The size of the subcell forming region is decreased, and the subcell sizes are increased at the crack plane.
- 4) The magnitude of the shear stress range at the crack tip is diminished. The proportionality of stress range to  $r^{-1}$  is approached more slowly.
- 5) Stress range experienced by the material has the form

$$\Delta\sigma = 2.26 \sigma_0 (A + Br)^{-.262}$$

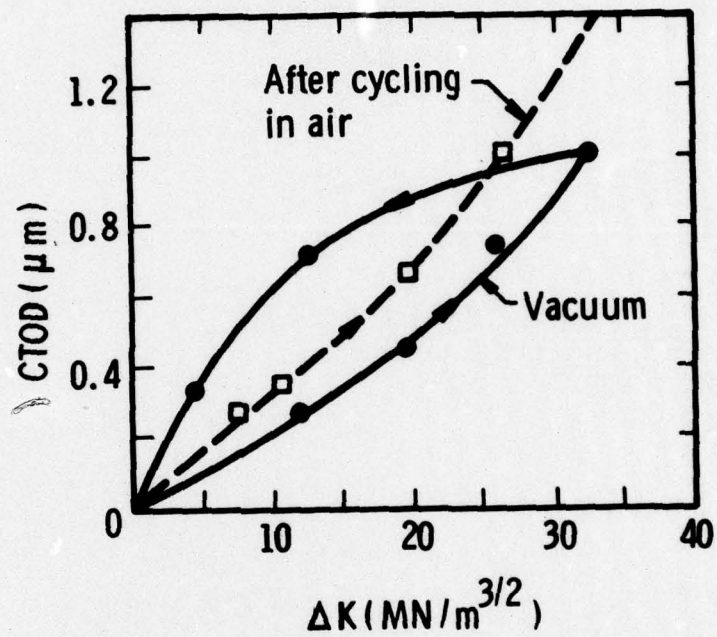


Figure 16. Crack Tip Opening Displacement As a Function of Stress Intensity Factor For a Crack Propagated in Humid Air vs Vacuum. From Photographs in Jono, et al (28). Arrows Denote Loading Path.

and strain range

$$\Delta\epsilon_p = 2/(A + Br)$$

where values of A and B are given in Figure 1 for both humid air and dry nitrogen environments.

- 6) The compressive stresses at the crack tip, for the unloaded condition, are probably reduced.
- 7) The energy expended in producing a unit area of crack is strongly reduced at low  $\Delta K$ , increasing to equal that for the dry nitrogen environment as  $\Delta K$  increases.
- 8) The presence of hydrogen at the crack tip probably a) reduces the Fe - Fe bond strength, and b) increases the cyclic and monotonic yield strengths of this low carbon steel.

This information is expected (a) to be useful from the viewpoint of mathematically modeling fatigue crack propagation, and seems (b) to fairly well delineate the mechanism of crack propagation and its alteration by environment. Moreover, it is possible to summarize the foregoing concepts into a fairly cohesive, albeit somewhat speculative model, as follows; although there may exist alternate explanations, there exists very little current information which is not supportive of the basic ideas developed below.

#### Fatigue crack propagation (no environmental effect)

At low values of  $\Delta K$ , fatigue crack propagation is exemplified by mixed mode crack opening (mode I + mode II). The mode I (tensile) opening drives the crack forward while the mode II (shear) displacement dissipates energy in the lattice through shear. As  $\Delta K$  increases, the amount of mode I increases, driving the crack even faster. Schematically, this may be represented as in Figure 17, which is a modified way of viewing a similar concept originating with Tomkins and Wareing.<sup>(31)</sup>

The material at the crack tip responds to the mode of crack opening by shearing in one or more shear bands. The number of shear bands and the angle of the shear band to the loading axis depend on a number of factors including the angle of the cracking plane to the loading axis and the magnitude of  $\Delta K$ . As  $\Delta K$  decreases, the path of the crack becomes much more irregular, so as the threshold is approached, the energy required for producing a unit area of crack (projected onto a plane perpendicular to the loading axis) increases.

#### The environmental effect

The major effect of environment is to alter the mix of opening modes, causing there to be an increase in the mode I (tensile) magnitude for a value of  $\Delta K$ . Since the shear sustainable by the material is lowered, the number of shear bands is increased, with a decrease in intensity of strain in each. The shearing bands also have a decreased length owing to their number. CTOD for a fixed strain at the crack tip is increased for a value of  $\Delta K$  because of the increased mode I opening and accompanying greater number of less intense shear bands.

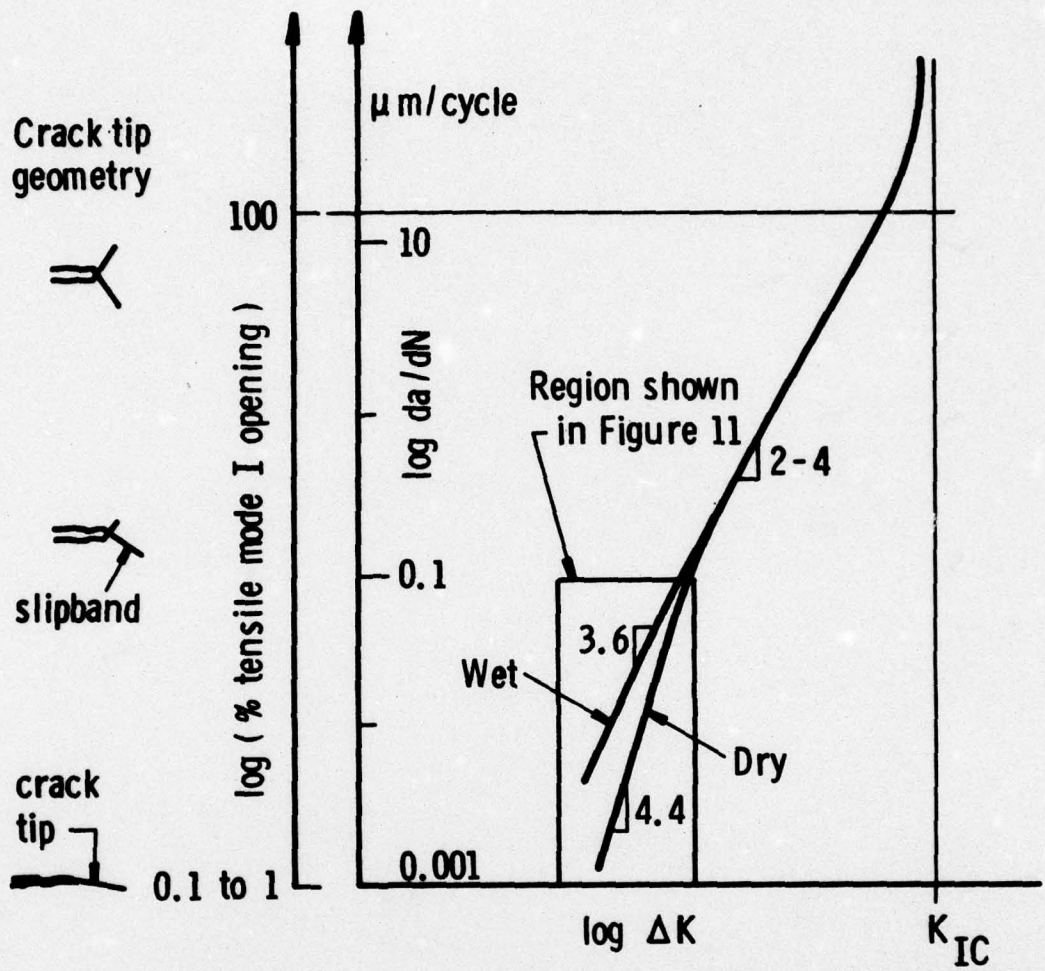


Figure 17. Schematic of the Relationship Between Crack Opening Mode Mix and the Parameters of Fatigue Crack Propagation

Hydrogen in the lattice, which may come from the catalyzed dissociation of  $H_2O$  in the presence of Fe by the mechanism described by Dwyer, Simmons and Wei(32) probably is carried into the lattice by a combination of diffusion(33) and dislocation sweep in(34). The effect of this lattice hydrogen, then, is probably a combination of (a) lowering the energy of the Fe - Fe bond, making the rupturing process easier, thus requiring less mechanical input of energy, and (b) increasing the resistance to plastic flow in the material. This latter effect concentrates the effect of strain; thereby reducing the volume of plastically deformed material and preventing some of the strain at the crack tip in individual shear bands. Thus, the energy required for cracking is reduced. The reduction of strain magnitude in each shear band decreases the requirement for reversed shear on the unloading cycle, which lowers the compressive stress at the crack tip in the unloaded condition. This implies that the crack tip begins to open at a reduced load on the tensile portion of the cycle, so that a greater CTOD and crack growth per cycle would be expected.

## REFERENCES

1. D. L. Davidson and J. Lankford, Jr. "Determination of the Energy of Fatigue Crack Propagation and Its Alteration by Wet Air," Environment Sensitive Fracture of Engineering Materials, AIME, (in press).
2. H. Abdel-Raouf, P. P. Behham and A. Plumbtree, Can. Met. Quart. **10**, 87 (1971).
3. H. Abdel-Raouf, A. Plumbtree and T. H. Topper, ASTM STP 519 ASTM, 28-57 (1973).
4. F. V. Lawrence and R. C. Jones, Met. Trans. **1**, 367 (1970).
5. D. L. Davidson, Scanning Electron Microscopy, 1977, **1**, IITRI, Chicago, 431 (1977).
6. D. L. Davidson and J. Lankford, Jr., Fracture 1977 2, ICF4, U. Waterloo Press, Waterloo, Ontario, 897 (1977).
7. O. K. Chopra and C. V. B. Gowda, "Substructural Development During Strain Cycling of Alpha Iron," Univ. of Waterloo, Civil Engineering Dept. Report under AFOSR Grant 17-2120, June, 1974.
8. K. Herz, H. Mughrabi and M. Wilkens, "Cyclic Deformation of Alpha Iron Single Crystals in the Saturation Regime as a Function of the Strain Rate," Arbeitsbericht MPI/77/P3, Max-Planck-Institut für Metallforschung, Stuttgart, Germany, 1977.
9. D. L. Holt, Journal of Applied Physics, **41**(8), 3197-3201 (1970).
10. D. Kuhlmann - Wilsdorf, "Workhardening in Tension and Fatigue," Ed. A. W. Thompson, AIME, 1977, p 7.
11. H. Mughrabi, K. Herz and X-Stark, Acta Met., **24**, 659 (1976).
12. R. W. Langraf, "Cyclic Stress-Strain Response in Commercial Alloys," in Workhardening in Tension and Fatigue, AIME, New York, p 240 (1977).
13. D. L. Davidson, J. Lankford, T. Yokobori and K. Sato, Internat. J. Fract. **12**(4), 579-585 (1976).
14. G. V. Karpenko, N. Ya Yarmchenko and M. M. Shved, Soviet Materials Science, **7**(3), 304-306 (1971), Translation Oct 1973.
15. S. Asano and R. Otsuka, Scripta Met., **10** 1015-1020 (1976).
16. H. Kimura, H. Matsui and S. Moriya, Scripta Met., **11**, 473-474 (1977).
17. I. M. Bernstein, ICF4, Waterloo, Ontario, during a discussion to the session on effect of environment on fatigue mechanisms, 1977.

REFERENCES (Continued)

18. E. Lunarska, A. Zielinski and M. Smialowski, Acta Met, 25, 305-308 (1977).
19. J. Schijve, "Analysis of the Fatigue Phenomenon in Aluminum Alloys", PhD Thesis at the Delft University of Technology, 1964, Appendix B. (Also NLR-TRM 2122, National Aeronautical Research Institute, Amsterdam, 1964).
20. J. Awatani, K. Datagiri and T. Shiraishi, Met. Trans. 7A, 804 (1976).
21. J. Awatani, K. Katagiri and H. Nakai, Met. Trans. 9A, 111-116 (1978).
22. K. Katagiri, J. Awatani, A. Omura, K. Kuyanagi and T. Shiraishi, ASTM Symposium "Fatigue Mechanisms" Kansas City, May 1978, To be published.
23. J. R. Rice and M. A. Johnson, "Inelastic Behavior of Solids", ed. by Kanninen, et al, McGraw Hill Book Co., New York, 641 (1970).
24. K - H. Schwalbe, Trans ASME, J. Eng. Mat and Tech, 99(4), Series H, 186-188 (1977).
25. J. R. Rice, "Fatigue Crack Propagation", ASTM STP 415, American Society Testing Materials, 247-309 (1967).
26. G. T. Hahn, R. G. Hoagland and A. R. Rosenfield, Met. Trans. 3, 1189-1202 (1972).
27. S. Taira and K. Tanaka, Eng Fract Mechanics, 4, 925-938(1972).
28. M. Kikukawa, M. Jono, and M. Adachi, "Direct Observation and Mechanism of Fatigue Crack Propagation", to be published in Fatigue Mechanisms, ASTM STP.
29. D. L. Davidson, "Fatigue Crack Tip Displacement Observations", J. Mater Science (in press).
30. J. Schijve, Eng Fract Mechanics, 10, 359-370 (1978).
31. B. Tomkins and J. Wareing, Metal Science, 11(8 and 9), 414-424 (1977).
32. D. J. Dwyer, G. W. Simmons and R. P. Wei, Surface Science, 64, 617-632 (1977).
33. R. P. Gangloff and R. P. Wei, Met Trans, 8A, 1043-1053 (1977).
34. J. K. Tein, R. J. Richards, D. Buck, and H. L. Marcus, Scripta Met, 9, 1097-1101 (1975).